Nuclear Engineering and Design 424 (2024) 113298

Contents lists available at ScienceDirect

Nuclear Engineering and Design

journal homepage: www.elsevier.com/locate/nucengdes

LES of the upper plenum of the liquid metal fast reactor under the forced flow conditions

Ashish Saxena *, Matthew Falcone, Shuisheng He

Department of Mechanical Engineering, University of Sheffield, Sheffield, United Kingdom

ARTICLE INFO

Keywords:
Liquid Metal Fast Reactors
Lead-Bismuth Eutectic
Forced Convection
Thermal Stratification

ABSTRACT

A Large Eddy Simulation (LES) of the upper plenum of the E-SCAPE (European SCAled Pool Experiment) facility under the normal operations has been conducted to gain deeper insights into the thermal hydraulics phenomena in liquid metal fast reactors (LMFRs). The results unravel the overall flow features in the upper plenum, the thermal instability in the above core structure region and the impact of the jets from the barrel holes on the large flow circulation and thermal mixing.

The above core structure region is represented using a homogeneous porous model. It is shown that during the normal operations, most of the hot stream of the lead bismuth eutectic (LBE) from the core center rises to the top and disperses from the upper barrel holes. Conversely, the cold LBE spread out from the lower barrel holes. Mixing between the two streams only affect the fluids leaving from the middle heights demonstrating limited mixing. These jets help to create a large circulation in the upper plenum region which prevents any thermal stratification. At the interface between the hotter and colder streams, there are unsteady large-scale structures resulting in a mixing layer in the thermal field. This strong mixing is not conventional turbulence and potentially cannot be captured by Reynolds Averaged Navier Stokes average (RANS) modelling.

The flow in the upper plenum is dominated by the influences of the different types of jets, which include some free jets issued horizontally or angled upwards and some jets impinging onto the structures in the plenum. The jets overall behave similar to 'standard' jets, though significant interactions between the top and bottom jets and the background circulations have strong influences at later stages of the jets, typically after four jet diameters leading to the jets not reaching self-similarity. In addition, the turbulence that is observed in the upper plenum is largely generated by the jet flows and hence the distribution of turbulence is very non-uniform. Away from the jets, turbulence is minimal with the mixing largely driven by the large-scale circulation.

1. Introduction

Liquid Metal Fast Reactors (LMFRs) are a prospective nuclear reactor design with characteristics that make them a favorable choice over existing designs. The advantages of these reactors include improved safety characteristics resulting from the properties of the liquid metal coolant, such as the high boiling point and thermal conductivity of liquid metals, which provide a degree of passive safety. These designs can also offer higher thermal efficiency and fuel utilization. However, there are challenges associated with the introduction of such designs, some of which occur in the upper plenum, particularly in off-design conditions. These include thermal stratification and thermal striping, which can induce stresses and fatigue within the components of the reactor (Roelofs et al., 2019). Beyond these design challenges, there are also challenges associated with computational fluid dynamics (CFD) modelling (Roelofs et al), which cannot be reliably represented using standard models. These issues are exacerbated in cases of natural and mixed convection, where phenomena such as stratification are often incorrectly predicted. As a result, there is a need for both high-fidelity simulation of, and experiments with, LMFRs to improve understanding of the physics of these flows and to validate computational tools for improved modelling.

Recently, studies have been conducted to investigate the thermal hydraulics phenomenon in LMFRs during the reactor transients. Scaled facilities have been used to study reactor core behaviors. The Belgian National Nuclear Research Centre, SCK-CEN has developed the E-SCAPE test facility, which is a 1:6 scale model of the future LMFR, MYRRHA (Multi-purpose hYbrid Research Reactor for High-tech Applications). Like MYRRHA, E-SCAPE uses lead bismuth eutectic (LBE) as the primary

* Corresponding author.
E-mail addresses: ashish.saxena@sheffield.ac.uk (A. Saxena), m.falcone@sheffield.ac.uk (M. Falcone), s.he@sheffield.ac.uk (S. He).

https://doi.org/10.1016/j.nucengdes.2024.113298
Received 4 February 2024; Received in revised form 8 April 2024; Accepted 3 May 2024
Available online 10 May 2024

Nomenclature

Abbreviations

ACS	Above core structure
CFD	Computational fluid dynamics
DNS	Direct numerical simulation
HX	Heat exchanger
IVFHM	In-vessel fuel handling machine
LBE	Lead-bismuth eutectic
LES	Large eddy simulation
LMFR	Liquid metal-cooled fast reactor
PP	Power pumps
RANS	Reynolds-averaged Navier-Stokes
SD	Silicon-doping devices
SGS	Sub-grid scale
TKE	Turbulence kinetic energy
UP	Upper plenum
WALE	Wall-adapting local eddy viscosity

Greek Symbols

α	Thermal diffusivity
β	Thermal expansion coefficient
ρ	Fluid density
$\in$	TKE dissipation
μ	Dynamic viscosity
ν	Kinematic viscosity
ν_t	Eddy kinematic viscosity
α_t	Eddy thermal diffusivity
ϕ	Porosity
λ	Thermal conductivity
τ_{ij}^r	Sub-grid residual stress tensor
$\prod_i^r$	Sub-grid scale heat flux

Roman Symbols

C_p	Specific heat
d	Diameter of barrel holes or jets
g	Gravity
U	Instantaneous velocity
$\overline{U}$	Mean velocity
T	Instantaneous temperature
$\overline{T}$	Mean Temperature
t	Time
S_i	Source term in the i direction
P	Pressure
Pr_t	Turbulent Prandtl number
x_i	Coordinate in the i direction

Other Symbols

$(\sim)$	LES filtering operation

coolant. The E-SCAPE facility has been developed to understand the thermal hydraulics phenomenon in the plenum and for validating the computational tools (Tichelen et al., 2015). Tichelen and Mirelli, (2019) conducted experiments on the E-SCAPE facility and reported that thermal stratification occurs at a low flow rate (natural convection) and thermal mixing occurs at a high flow rate (forced convection). For analyzing the flow and heat transfer in the E-SCAPE facility, different institutes such as NRG, SCK-CEN, and VKI developed RANS models of the entire main vessel using different CFD software, including STAR-CCM, ANSYS CFX, and OpenFOAM during normal operations (Visser et al., 2020). Visser et al., (2020) validated the NRG model, which used standard $k-\in$ model, incorporating a higher value of turbulent Prandtl number $(Pr_t = 2.0)$, in various flow rates. Their numerical results compared reasonably well with the experimental data. Studies on the thermal stratification in the upper plenum of the simplified model of the MONJU reactor under steady state and transient conditions have also been reported in the literature (Choi et al., 2013; Wang et al., 2020). In this direction, Choi et al., (2013) reported that the numerical results, which were performed by using CFX-13, were in good agreement with the experiments under steady state conditions. However, it was only capable of predicting the initial stages of a turbine trip transient, with the model failing to predict the stratification once natural convection dominated. In a recent study, Wang et al., (2020) simulated the upper plenum of the MONJU reactor under steady state and shutdown transient conditions. They discussed the detailed flow field above the core outlet and the influence of a barrel surrounding the upper plenum on thermal stratification during the shutdown transient, finding that it improved thermal mixing in the plenum.

Existing literature encompasses high-fidelity simulations specifically large eddy simulations (LES) focused on flow configurations relevant to nuclear reactors across various convection regimes. Notably, these simulations have provided valuable insights into the behavior of liquid metals compared to ordinary fluids. LES was used by Choi et al., (2015) and Chacko et al., (2011) to understand thermal striping in the upper plenum of the Prototype Generation IV sodium-cooled fast reactor (PGSFR) developed at the Korean Energy Research Institute. In these studies, it was demonstrated that LES is more capable of predicting thermal striping than RANS because it can predict the temporal variations of the temperature. High fidelity simulation for the turbulent forced and mixed convection cases of LBE around rods bundle has been carried out by Angeli et al., (2019). In their study, they observed a mean secondary flow that generates a circulatory motion of the same size as the elementary flow cell. To understand the phenomenon of buoyant stream mixing which holds significance in liquid metal fast reactors, Fregni et al., (2019) performed direct numerical simulation for a non-isothermal triple jet (cold-hot–cold) configuration at low Prandtl number. Their discussion encompassed several phenomena including the effect of buoyancy at low Prandtl number fluids, interaction between jet of different temperature and the presence of the mixing layers. Since high fidelity simulation can accurately predict fundamental liquid metal flows, including highly oscillatory mixing jets, it is a preferred method understanding the physical phenomena in liquid metal fast reactors and can provide high spatial and temporal resolution of the flow fields enabling detailed study of the flow physics.

From the literature it is evident that turbulence modelling for the liquid metal cooled fast reactor has several challenges. These challenges include dealing with the complexities inherent in the system, which is characterized by various flow regimes and the utilization of a low Prandtl number working fluid (Grötzbach, 2013; Roelofs et al., 2015). The challenges associated with the modelling of low Prandtl number fluids result from the violation of the Reynolds analogy, which is used in eddy diffusivity approaches to modelling the turbulent heat flux, where the eddy diffusivity, α_t is assumed to be approximately equal to the eddy viscosity leading to the turbulent heat flux, $\langle u_i' T' \rangle = -\frac{\nu_t}{Pr_t}\frac{\partial T}{\partial x_i}$, with the turbulent Prandtl number, $Pr_t \approx 1$. In liquid metal flows, Pr_t typically significantly deviates from one leading to incorrect predictions of the turbulent heat flux. Shams et al., (2014) discussed the limitation associated with the eddy diffusivity approach in modelling of turbulent heat flux for Rayleigh-Benard convection. They evaluated and further calibrated the algebraic turbulent heat flux model of Kenjeres et al., (2005) in the commercial code STAR-CCM+, which does not rely on the Reynolds analogy, improving predictions of the mean temperature for flow regimes ranging from natural to forced convection and was found to be applicable at Prandtl numbers typical of liquid metals. High fidelity

simulations of turbulent heat transfer in channel flow at a range of Prandtl and Reynolds numbers were carried out by Kawamura et al., (1999). In their study, they demonstrated a significant impact of the Reynolds number on the turbulent Prandtl number, particularly for a fluid with a lower Prandtl number.

From the literature, it is apparent that there has only been limited scale resolving simulations of liquid metal fast reactors. In this context, a large eddy simulation of the E-SCAPE facility has been carried out. The purpose of the study is to generate trustworthy detailed information to support experimental endeavors, advance the understanding of the complex flow phenomena in different regimes of the upper plenum of the E-SCAPE facility, and create a database for the development of advanced nuclear reactor systems using liquid metal as a coolant.

2. Methodology

The E-SCAPE facility is a 1/6-scale thermal hydraulic model of the MYRRHA reactor, employing LBE as a coolant in a pool-type design. In the E-SCAPE facility, the heat exchangers and the power pumps have been integrated into the external cooling circuit as shown in Fig. 1(a). Fig. 1(b) provides a comprehensive view of the plenum and all components of the E-SCAPE facility. The pool-type facility comprises two power pumps (PP), two in-vessel fuel handling machines (IVFHM), two silicon doping devices (SD), and four mock-up heat exchangers (HX). The mock-up heat exchangers (5 in Fig. 2) resemble hollow tubes with slotted inlets (green rectangles) and represent where the heat exchangers would be in MYRRHA. In E-SCAPE, the actual heat exchangers are located in the external circuit. E-SCAPE also includes a mock-up core and an 'above core structure region' (The ACS region is depicted in Fig. 1(b)). During normal operation, cold LBE is pumped from the lower plenum to the upper plenum through the core while being heated. The flow spreads out in the radial direction into the upper plenum through the barrel holes as jets. The flow exits from the upper plenum through the four mock-up heat exchangers (5 in Fig. 2(a)) for the secondary external cooling circuit. E-SCAPE's mock-up core is an electric heater made up of seven annular rings, with the six inner rings forming the 'active' region where most of the heating occurs. In contrast, the outer ring of the core is known as the 'bypass' and is unheated in the case presented in this study, with cold coolant passing directly from the lower plenum to the upper plenum.

The objective of the present study focuses on the upper plenum of the E-SCAPE facility and hence only the upper plenum was modeled. Fig. 2 (a) shows the upper plenum of the E-SCAPE facility along with all its components (components are listed in the caption of Fig. 2). Fig. 2 (b & c) offer a top view and a quarter view of the model, respectively.

The ACS region is covered by a perforated tube called the barrel wall, which has five rows of barrel jets (as shown in the Fig. 2(a) with the number 1 notation). The area surrounding the ACS region is known as the upper plenum region. The rounded barrel holes enable the flow of coolant from the ACS region into the upper plenum region. The hot stream originating from the center of the core and the colder stream bypassing and surrounding the core interact within the above core structure region and disperse through the barrel jets.

Several assumptions have been incorporated for the modelling of the E-SCAPE facility specifically for the ACS region. The core outlet of the E-SCAPE facility serves as the inlet for the CFD model. The core of the E-SCAPE facility consists of seven annular shells with varying heating profiles, leading to non-uniform mass flow rates and temperatures at the core outlet, which can be observed in the experimental results (Tichelen and Mirelli, 2019). These outlets introduce jets into the above core structure region. In the present analysis, the inlets are simplified by considering just an 'active inlet' and a bypass inlet with a uniform mass flow and temperature in each inlet. This is similar to the approach of Toti et al., (2018), which also modelled the inlet as an active and bypass inlet. More details of how the mass flow and temperatures were determined are presented in section 2.2.

In addition to this, the ACS is modeled using a simple porous media approach, so that the pressure losses from the ACS can be represented to allow an appropriate mass flow distribution through the barrel holes whilst ensuring that the simulations remain computationally feasible. In a similar approach to that of Toti et al., (2018) and Koloszar et al., (2017), an explicit momentum source term was added to account for the pressure losses in the ACS region. Source terms are included based on the inertial term of Forchheimer's equation. The resulting Forchheimer coefficients were calculated using correlations for the pressure loss in rod bundles (Todreas and Kazimi, 1990; Todreas and Kazimi, 2001). The planes where the results are presented are depicted in Fig. 2 (d, e and f) for the convenience of the readers.

The filtered conservation equations for mass, momentum, and energy, are solved:

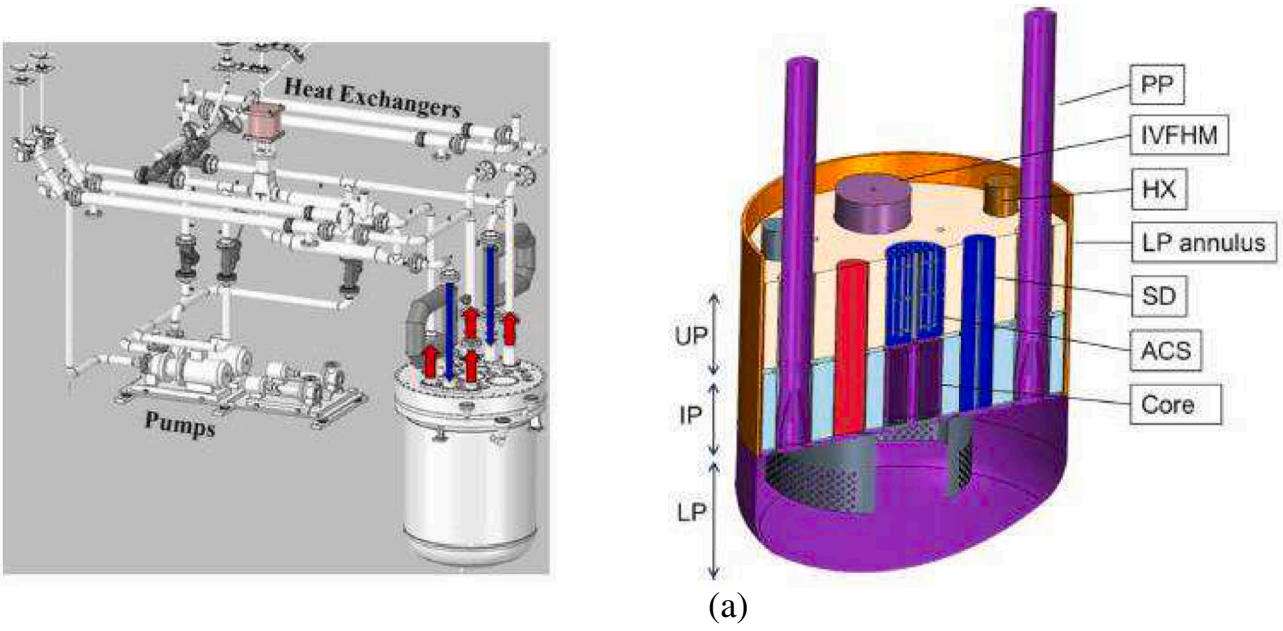

Fig. 1. (a) Schematic of the E-SCAPE facility with external cooling circuit; (b) Components of the E-SCAPE pool clipped view from (Visser et al., 2020).

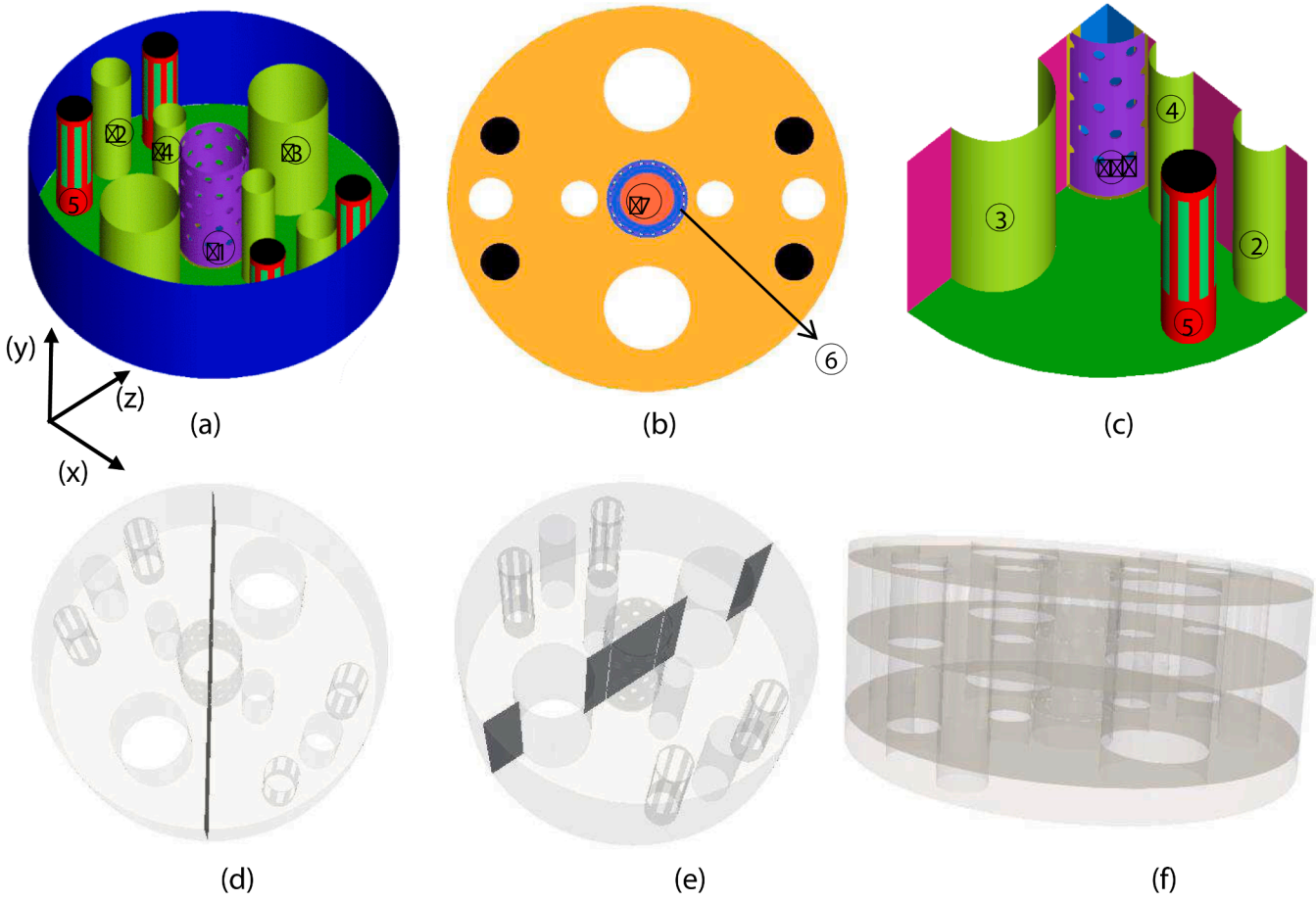

Fig. 2. (a) Schematic of the upper plenum of E-SCAPE model; (b) Top view; (c) Quarter representation; (1) Barrel wall; (2) Power pump; (3) In-vessel fuel handling machines (IVFHM); (4) Silicon-doping devices; (5) Heat exchanger; (6) Bypass inlet; (7) Active inlet; (d, e and f) planes where the results are presented; (d) free jet in the direction of the heat exchangers; (e) interacting jet in the direction of IVFHM; (f) horizontal planes; plane-1 is located near the bottom at y = 0.1 m; plane-2 is positioned at the middle at y = 0.28 m; plane-3 is situated near the top surface at y = 0.455 m. Coordinate system corresponds to (a): x in the direction of the silicon doping device; z in the direction of the IVFHM; y in the direction of the height of the upper plenum region.

$$\frac{\partial \rho\phi}{\partial t} + \frac{\partial \rho\phi\widetilde{U}_i}{\partial x_i} = 0 \tag{1}$$

$$\frac{\partial \rho\phi\widetilde{U}_i}{\partial t} + \frac{\partial \rho\phi\widetilde{U}_i\widetilde{U}_j}{\partial x_j} = -\frac{\partial \phi\widetilde{P}}{\partial x_i} + \frac{\partial}{\partial x_j}\left(\mu\left(\frac{\partial \phi\widetilde{U}_i}{\partial x_j} + \frac{\partial \phi\widetilde{U}_j}{\partial x_i}\right) - \phi\tau_{ij}^{r}\right) + \phi\rho\mathbf{g} + \phi S_i \tag{2}$$

$$\frac{\partial \rho C_p\phi\widetilde{T}}{\partial t} + \frac{\partial \phi\widetilde{U}_i\widetilde{T}}{\partial x_i} = \frac{\partial}{\partial x_i}\left(\phi k\frac{\partial \widetilde{T}}{\partial x_i} - \phi\prod_i^{r}\right) \tag{3}$$

Here the properties are of the LBE; P is the flow pressure; t is the time; x_i is the coordinate in the i direction; ϕ is the volume porosity; $(\widetilde{\ })$ is the LES filtering operation. S is the source term from the implicit ACS model. τ_{ij}^{r} is the sub-grid residual stress tensor which is determined using the WALE model. $\prod_i^{r}$ is the sub-grid scale heat flux determined using the simple gradient diffusion hypothesis (SGDH) using the subgrid-scale (SGS) viscosity calculated through the WALE model, which Yahya et al., 2012 suggested was well-suited for LES in complex geometries. The open-source CFD solver Code_Saturne V6.0.0 (Code_Saturne, 2019) was used. Code_Saturne's default values for the WALE model constant and the SGS Prandtl number for the SGS heat flux are used, with, C_w = 0.25 and Pr_{SGS} = 1. The Second-Order Linear Upwind (SOLU) scheme was used to discretize the governing equations. A time step of 5×10^{-4}s was used, which ensured that the CFL was less than one at most locations, and thus maintained simulation stability. The SIMPLEC pressure–velocity coupling algorithm was used with a relaxation factor of 0.5.

The LES simulation begins from an initially fully developed RANS simulation. The LES results are collected after the simulation has reached the statistically steady state, i.e., when the averaged values at the monitored locations remain unchanged.

2.1. Grid

The ICEM-CFD has been used to create a mostly structured mesh. However, an unstructured tetrahedral mesh with inflation layers has been used to mesh the complex geometry around the barrel wall, with a hexahedral block structured mesh used for the remainder of the domain, and with 'O-grids' around the cylindrical surfaces to reduce numerical diffusion. The mesh and blocking are shown in Fig. 3, noting the unstructured and O-grid meshing in Fig. 3(c). A layer of pyramids was used to create a conformal interface between the unstructured and structured meshes. The total number of elements used for these simulations was 47 million. In the near-wall region the mesh is refined to ensure that the first cell center is placed well within the viscous sub layer, i.e., the dimensionless wall normal distance, y^+, is kept lower than 1 (confirmed by the simulation results).

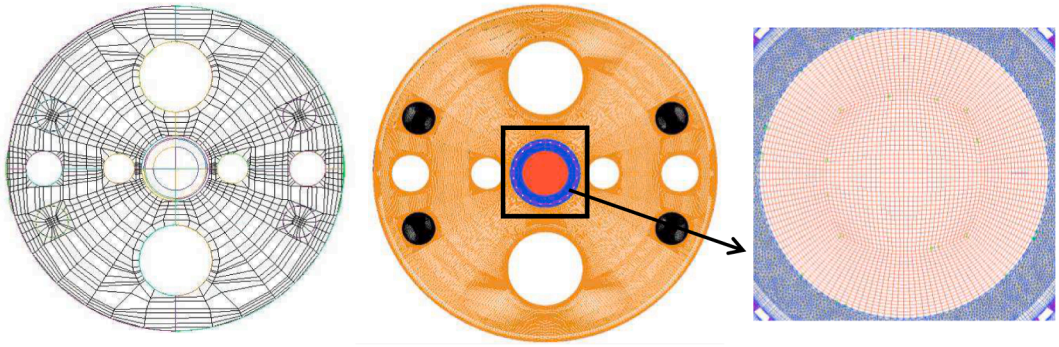

Fig. 3. Mesh methodology (a) O-grid; (b) Structured and unstructured mesh from the top view; (c) Zoom view of the unstructured and structured mesh in the bypass and active inlet region.

2.2. Boundary conditions

The boundary conditions are based on the experimental investigations conducted for the E-scape facility (Tichelen and Mirelli, 2019). The configuration simulated is corresponds to the forced convection case, labeled as F80%-P80%-BP0% in (Tichelen and Mirelli, 2019). The temperature for the active inlet was set at 190 °C and the bypass inlet temperature was set at 180 °C. These values were based on the experimental results, although due to the non-uniform temperature distribution at the core outlet, these are approximate with the temperature in the facility reaching a maximum of around 193 °C. The mass flow rates at each inlet were determined by taking the energy balance of the facility based on the nominal core power (66.4 kW), mass flow rate (93.2 kg/s) and the active and bypass inlet temperatures. This leads to a mass flow rate of 45 and 48.2 kg/s for the active and bypass inlets respectively. This approach differs from Toti et al., (2018, which used a system code model of the rest of the facility to determine the core outlet mass flow rates and temperatures. In the present model, the core outlet jets are simplified by using a homogenized inlet where the mass flow for each inlet is distributed over each inlet's area. An outlet (black discs in Fig. 2) is located inside each mock-up heat exchanger, with a pressure boundary condition imposed.

The LBE free surface and cover gas are not explicitly modelled. Instead, the free surface was modelled with a symmetry boundary condition, resulting in no shear stress there. The viscosity of argon is ≈100 times smaller than LBE thus it can be assumed the motion of the plenum is not strongly affected by the cover gas. The height of the free-surface is chosen based on available literature. In the paper by Tichelen and Mirelli, (2019), it was noted that the height of the upper plenum is approximately ≈760 mm, including the core region under the forced convection case. Results from Visser et al., (2020) indicate that that the height of the core region is around ≈325 mm, indicating that the height of the free surface or the upper plenum region is approximately (760——325 = 435 mm). The walls in the model are considered adiabatic with Visser et al., (2020) indicating that the total heat loss to the surroundings in this case was approximately only 3 %. Much of the heat transfer in the forced circulation case is driven by the convection of the jets with the influence of conduction through solid components likely to be small. As a result, conjugate heat transfer effects are not considered for the solid components within the domain such as the barrel wall. The Batten method (Pope, 2000; Code_Saturne, 2019) was used to generate turbulent inflow conditions for the facility.

2.3. Thermo-physical properties

The correlations developed by Sobolev (Sobolev, 2011) were used to determine the variations in all physical properties of LBE. These comprehensive variations are documented in the listed Table 1.

Table 1
Thermo physical properties of the LBE.

Properties	Value (Unit)
Density	$11065–1.293 \times T$ (Kg/m^3)
Specific heat	$164.8 – 3.94 \times 10^{-2} \times T + 1.25 \times 10^{-5} \times T^2 – 4.56 \times 10^5 \times T^{-2}$ (J/kg•K)
Dynamic viscosity	$4.94 \times 10^{-4} \times \exp(754.1/T)$ (Pa•s)
Thermal conductivity	$3.284 + 1.617 \times 10^{-2} \times T – 2.305 \times 10^{-6} \times T^2$(W/m•K)

3. Results and discussion

The numerical methodology employed has been verified against the experimental results available in the literature [4 and 6] and the verification outcomes are detailed in section 3.1. Subsequently, the resolution quality for LES is evaluated in section 3.2. The comprehensive discussion on the overall flow behavior in the upper plenum region of E-SCAPE facility under the normal operations is discussed in section 3.3. Thereafter, the flow phenomena and mechanisms in the ACS region are discussed in section 3.4. The analysis of the flow patterns in upper plenum region and in the ACS region is based on the instantaneous and time-averaged fields at different planes of the upper plenum region. The turbulence quantities such as turbulent kinetic energy and turbulent heat flux are analyzed to improve the understanding of the turbulent mixing in the facilities. The characterizations of the rounded free jets originating from the barrel holes are explored in section 3.5. The behavior of the jets is discussed using both first-order and second-order statistics along the jet trajectories.

3.1. Validation

A comparison with experimental measurements is given in this section. Visser et al., (2020) presented experimental temperature measurements from various heights and locations in the upper plenum of the E-SCAPE facility for the conditions in the present work. Fig. 4 compares the present analysis and results given by Visser et al., (2020) for the forced convection case without bypass heating. From the results it can be seen that there are some discrepancies in between the numerical results, based on the LES simulations and the experiments. While both the experiments and simulations predict a relatively uniform temperature distribution with height, there is an offset in temperature values. The LES model indicates a temperature ≈185.3 °C, whereas the experimental measurement shows around ≈184.3 °C, indicating a ≈1°C offset between the numerical and experimental results. Several factors contribute to this offset. Firstly, the use of homogenized inlets rather than the core outlet jets that are present in the real facility. Secondly, the use of just an active and bypass inlet without considering the

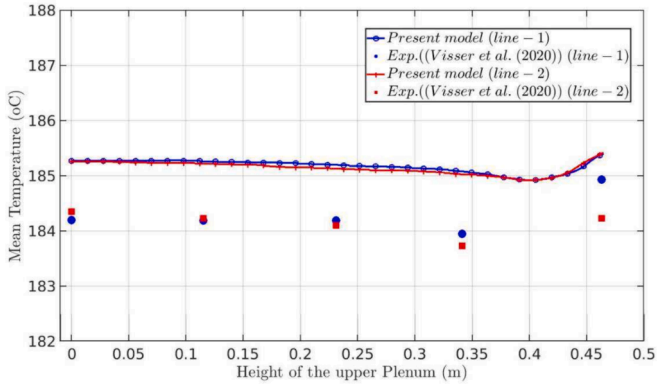

Fig. 4. Temperature distributions in the upper plenum region along the height of the upper plenum with comparison against the experimental measurements (Visser et al., 2020). Line-1 and line-2 are at different location in the upper plenum region.

nonuniformity of the mass flow and temperature in each inlet due to the differential heating in each core shell. Thirdly, the use of a porous media model of the ACS which would not be able to capture all aspects of the flow physics in the ACS potentially leading to different mixing characteristics in the ACS. The use of adiabatic conditions on the walls of the plenum would also be expected to contribute to the differences in temperature although the approximately 3 % heat loss (Visser et al., 2020) would mean that this effect probably only has a small influence. Nonetheless, the similar trends in the temperature profile at different locations suggests the overall flow characteristics in both cases are similar and that useful qualitative information about the flow physics can be obtained from the present results. It should be noted that experimental velocity data was not available, and that the temperature lacked spatial resolution meaning that a more comprehensive validation, particularly for the jets was not possible in the present study.

3.2. LES quality

The accuracy of the numerical results depends on the resolution of the LES. To examine the mesh quality of the LES results, the LES-IQ methodology has been used which was introduced by Celik et al. (Celik et al., 2005; Celik et al., 2009).

$$\text{LES\_IQ}_{\nu} = \frac{1}{1 + 0.05\left(\frac{2\langle\mu_{sgs}\rangle}{\langle\mu\rangle}\right)^{0.53}} \tag{4}$$

Here, $\langle\mu_{sgs}\rangle$ is the time-averaged SGS viscosity and $\langle\mu\rangle$ is the time-averaged molecular viscosity. In their studies, Celik et al. suggested that the LES is sufficiently resolved when the LES_IQ is greater than 0.8, indicating that the molecular viscosity contributes to 80 % of the dissipation. LES-IQ has been extensively utilized in various engineering applications, including isothermal flow and reacting flows. Importantly, it is considered a generic criterion and is not specific to a particular type of flow.

Fig. 5 shows the distribution of the LES-IQ at different location in the upper plenum region. From the results it is observed that the value of the LES-IQ is 0.95 across the whole domain and even higher close to the wall. This indicate that the LES is well resolved in the current simulation.

3.3. Overall flow behavior in the upper plenum region

The instantaneous and mean temperature and velocity over vertical planes in the direction of the heat exchangers (Fig. 2(d)) and in the direction of the in-vessel fuel handling machines (Fig. 2(e)) are presented in Figs. 6 and 7. The former is an example of a free jet and the latter an impinging jet. It is evident from Fig. 6 (a, b) and 7(a, b) that the hot fluid rises from the center active inlet reaching the free surface before spreading out through the upper barrel holes as high-momentum jets. The cooler LBE from the core bypass flows through the lower sets of barrel holes. The instantaneous and mean temperature contours indicate that the temperature is largely uniform across the plenum height indicating that there is sufficient mixing even at locations far from the jets. The reason for the emergence of a uniform temperature distribution in the upper plenum is revealed in Fig. 6(d) and 7(d), which shows the mean velocity contours in vertical planes along a free jet and in the direction of the IVFHM, respectively. The free jets from the barrel holes result in a large-scale circulation throughout the upper plenum under normal operations. Such behavior is not only driven from the strongest upper jets but also the inclined lower jets, which retain much of their upward momentum from the core.

The instantaneous and mean temperature distributions across the horizontal plane at different heights of the upper plenum are reported in Fig. 8. The horizontal planes are chosen in such a way as to observe the temperature distributions close to the bottom (near the inlet), middle, and close to the free surface of the upper plenum (Fig. 2 (f)). From Fig. 8 (a-1, a-2, and a-3), it is apparent that for the forced convection, there is a largely uniform temperature distribution in the upper plenum region. However, there is a slight non-uniformity, with some slightly cooler fluid in the region where the large circulation is blocked by the IVFHM. There is a non-uniform temperature distribution close to the barrel jets in the middle of the upper plenum region with some cooler fluid also noticed in Fig. 8 (a-2). This is caused by the cooler fluid transported by the lower jets, which are angled upwards as the fluid retaining significant upward momentum. This suggests that both the lower and the upper jets contribute significantly to the large-scale circulation in the forced convection case.

Fig. 9 illustrates the instantaneous and mean velocity distribution at different horizontal planes within the plenum. The impinging jets on the silicon doping devices and IVFHM present the potential areas of the thermal striping. It is also apparent that there is flow separation around

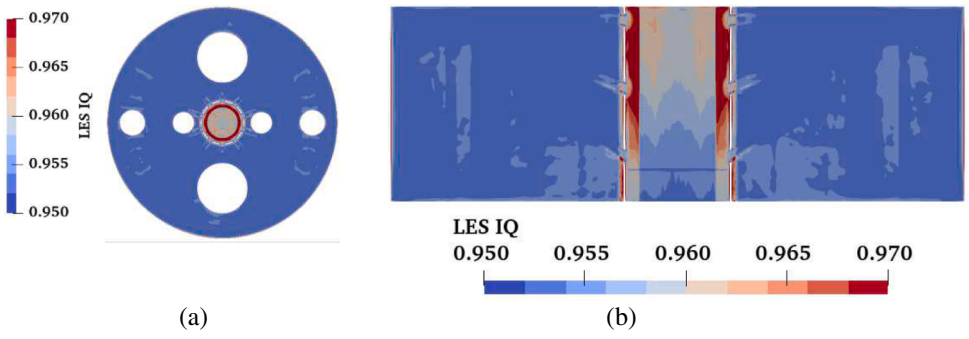

Fig. 5. LES-IQ distribution at different planes in the upper plenum region (a) Horizontal plane (near to the top) (b) Vertical plane in the free jet direction.

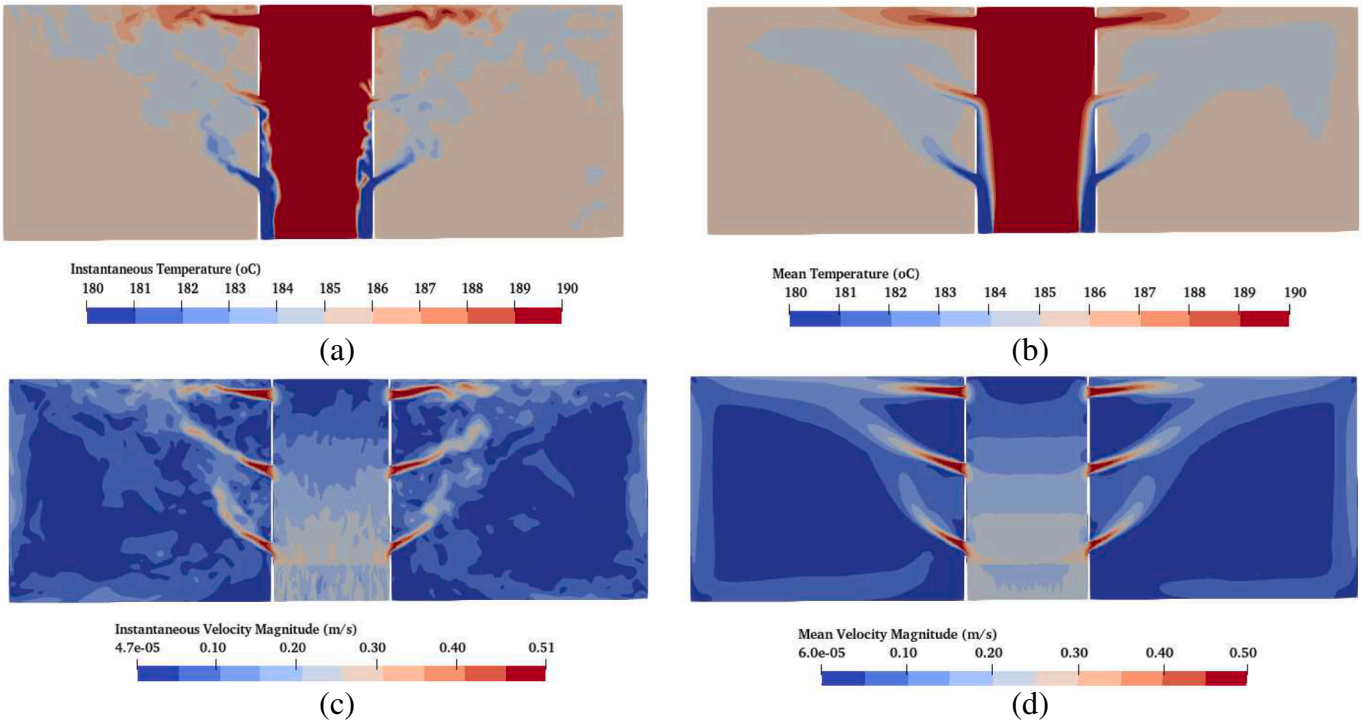

Fig. 6. Instantaneous and time averaged fields at a plane along the free jet direction; (a and b) Temperature profile, (c and d) Velocity magnitude profile.

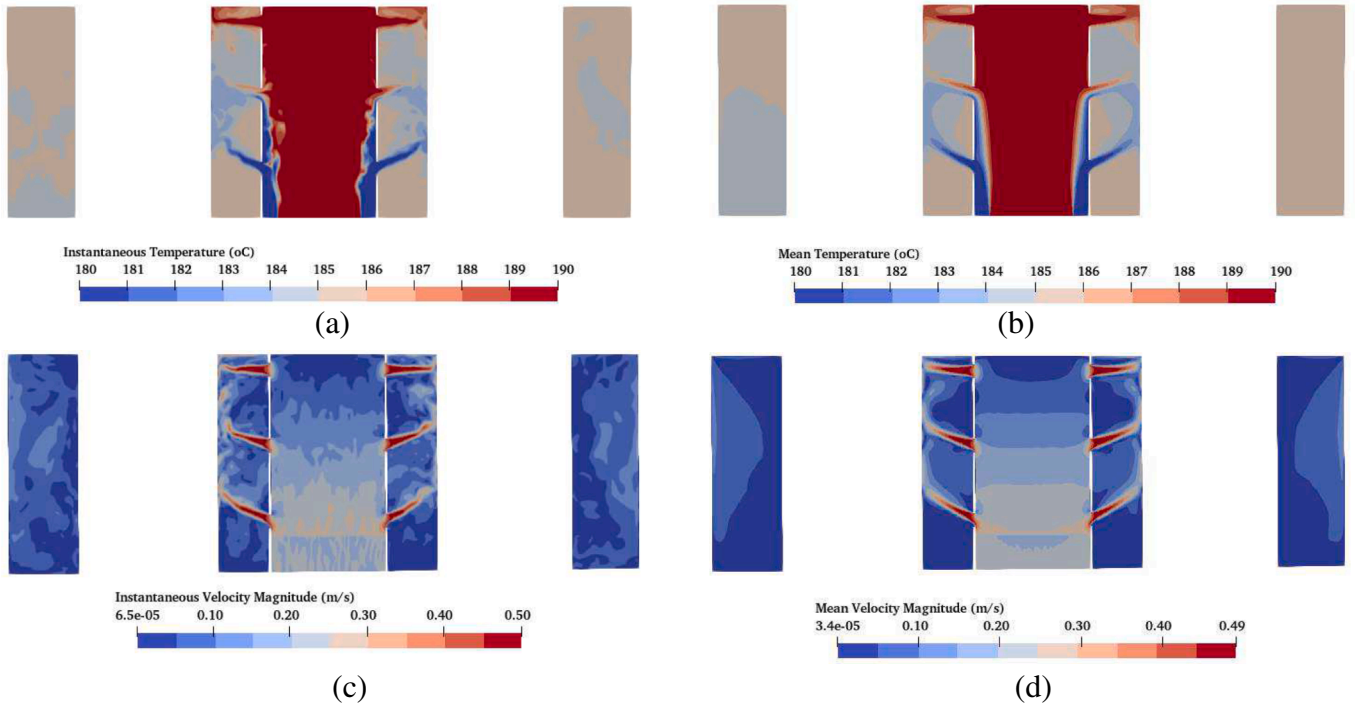

Fig. 7. Instantaneous and time averaged fields at a plane along the jet interacting with the IVFHM direction; (a and b) Temperature profile, (c and d) Velocity magnitude profile.

cylindrical surfaces, especially the heat exchanger tubes, pumps, and IVFHM. The jets situated near the top/free surface ((a-3) and (b-3) in Fig. 9) appear more powerful, potentially influenced by the upward momentum from the core, leading to higher horizontal velocity at the top.

The temperature and velocity distribution, based on the RANS simulation results presented in the appendix A. The results show that RANS appears capable of capturing many of the key phenomena in the forced convection case. This includes the uniform temperature observed in the upper plenum region, attributed to the presence of a large-scale circulation formed by the barrel jets. Additionally, the non-uniform temperature near the barrel holes suggests the influence of both the

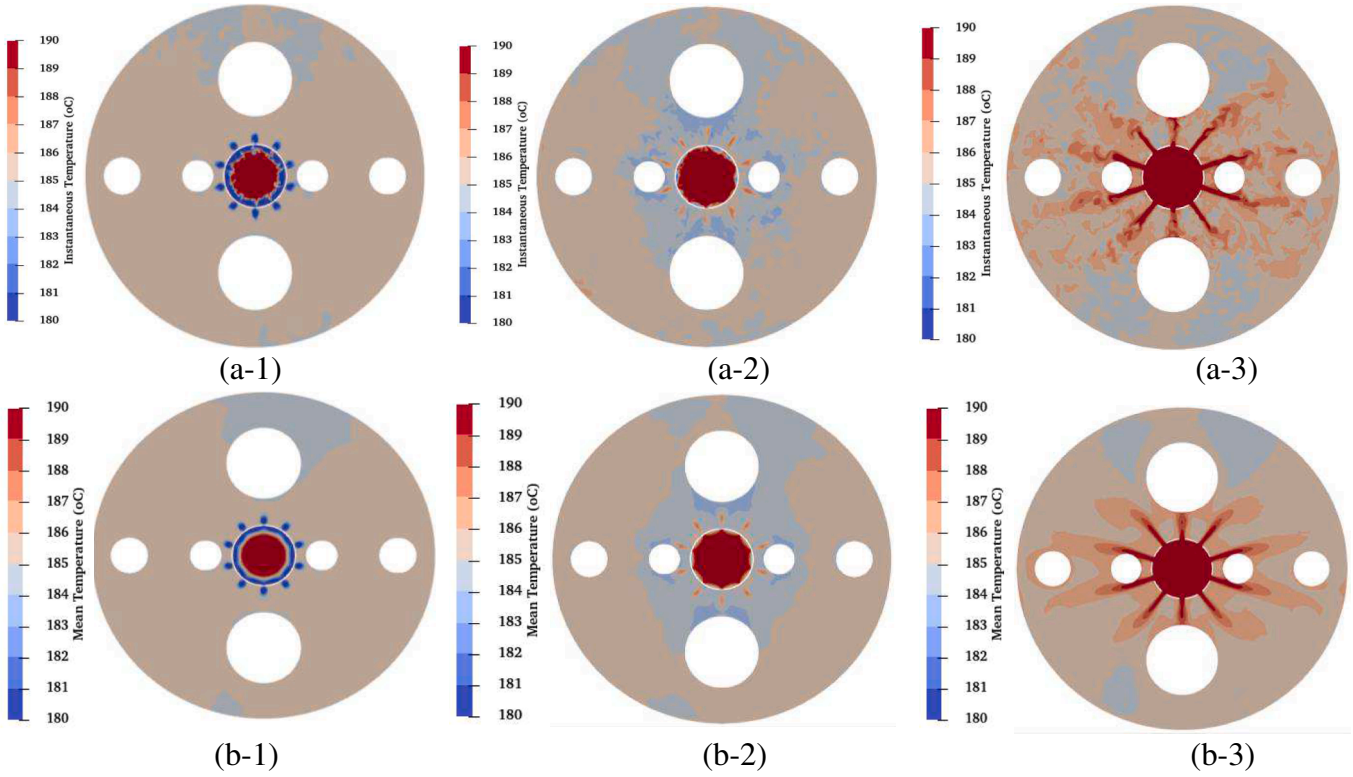

Fig. 8. Instantaneous and mean temperature distribution at different levels of the upper plenum. (a-1), (a-2) and (a-3) Instantaneous temperature; (b-1), (b-2) and (b-3) Mean temperature.

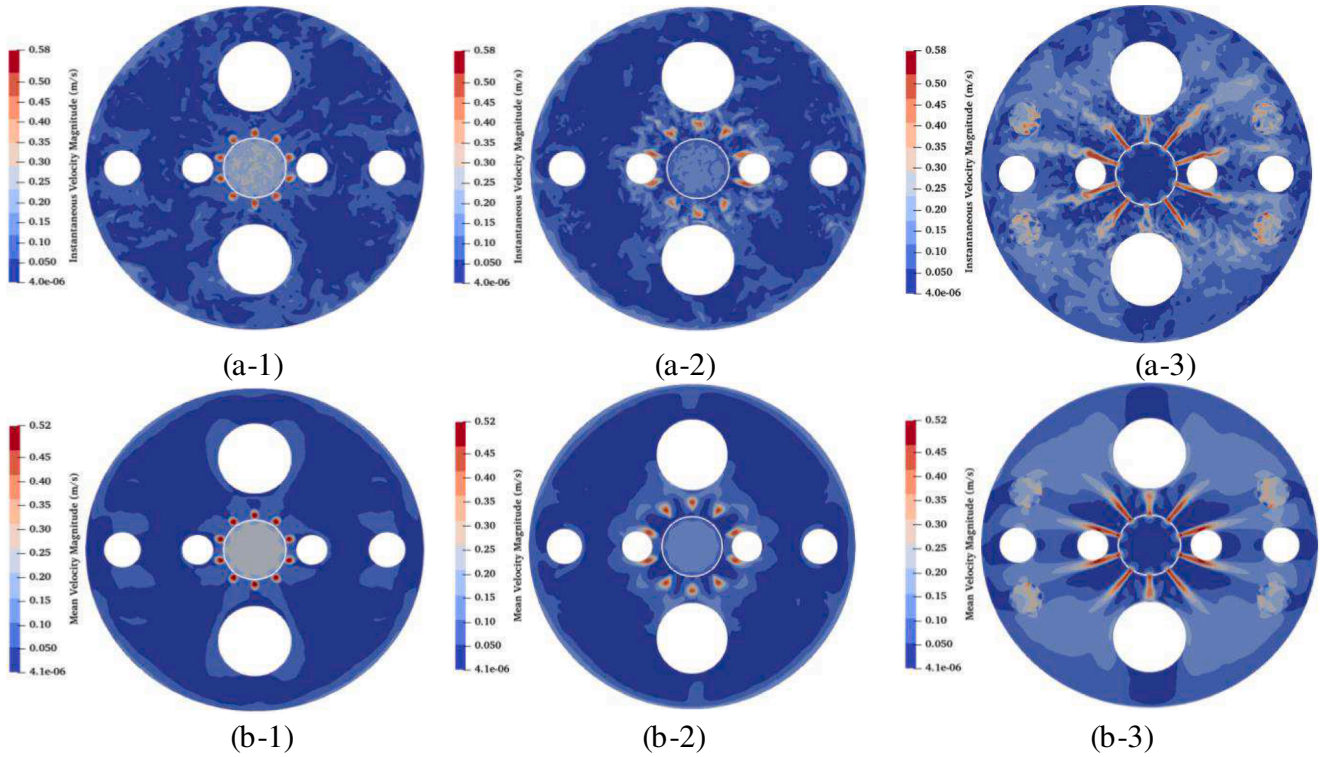

Fig. 9. Instantaneous and mean velocity distribution at different levels of the upper plenum. (a-1), (a-2) and (a-3) Instantaneous velocity; (b-1), (b-2) and (b-3) Mean velocity.

lower and upper jets in driving the large-scale circulation in the forced convection conditions.

The distribution of the turbulent kinetic energy (TKE) and the turbulent heat flux (THF) over the vertical planes in the direction of the IVFHM (Fig. 2(e)) and in the direction of the heat exchangers (Fig. 2(d)) are illustrated in Fig. 10. These distributions are used to understand the turbulent phenomena and the transport of heat via turbulence in the upper plenum region. From the TKE distribution it is noticed that the TKE is higher in the barrel jets from the upper sets of the barrel holes. As depicted in Fig. 10(b) it is noticed that the impingement of the jet at the IVFHM results in a region of high turbulence. The turbulent heat flux (Fig. 10(c) and 10 (d)) is also concentrated in the barrel jets with the peak occurring in the jets originating from the upper set of the barrel holes consistent with the larger velocity fluctuations there and reduced fluctuations for the lower jets. Away from the jets the turbulent heat flux reduces rapidly. A region of substantial turbulent heat flux is identified at the interface where the hot fluid from active inlet mixes with the cold fluid from the bypass.

3.4. Thermal instability in the above-core structure region

To begin with, we note again the simplifications of the modelling of the ACS in the present study, which most significantly include the use of homogenous porous medium model for the above-core structures and the uniform incoming flow representation of the jets flow from the core to this region. We do not expect these simplifications have significant impact on the upper plenum flow behaviors but the characteristics of the flow and mixing in the present model, the modelled ACS region are naturally different, in detail, from the flows in the real above-core structures. Nevertheless, the mixing of two concentric cold/hot streams in a homogenous porous medium is of interest in its own right, and in addition we trust that some features identified here are likely to be observable at least qualitatively in the ACS region too. With this note, we analyze the thermal instability of the modelled above-core structure region.

Fig. 11 depicts the instantaneous and mean temperature distribution in the above core structure region along the direction of in-vessel fuel handling machines and the silicon doping devices. The instantaneous temperature distribution reveals notable thermal diffusion within the above core structure region, attributed to the low *Pr* fluid. The instantaneous temperature fields provide useful insights on the thermal instabilities occurring in the above core structure region at the colder/hotter fluid interfaces. These appear to be typical Kelvin-Helmholtz (KH) instability occurring in high strain rate mixing layers. In contrast, the mean temperature distribution, as depicted in Fig. 11(b, d), and in Fig. 12, shows a smooth transition from the colder to hotter fluid within a thin layer. Clearly such smooth temperature distribution is a result of the average of highly unstable large scale unsteady structures. Such structures are well captured by the LES, but it is likely that RANS simulations will miss such details as having been shown in many previous studies of similar flows.

Fig. 13 (a & c) depict contour plots of the temperature variance within the above core structure region along with the direction of the silicon doping device and the in-vessel fuel machine handling. Conversely, Fig. 13 (b & d) presents the radial profile of the temperature variance at various height of the above core structure region following the same direction. The peaks observed in the radial distribution of temperature variance signify that the temperature is highly fluctuated in the region where the hot LBE is mixing with the cold LBE. The peaks gradually decreases and approach zero indicating that the temperature is stable in the upper part of the ACS, which is also shows by the temperature variance contour plots (Fig. 13(a) and 13(c)).

3.5. Characterization of rounded jet in the free direction

The jets through barrel holes play an important role in shaping the flow dynamics and thermal mixing in the upper plenum. The jets are sub divided into two categories: free jets when they do not interact with any components and interacting jets when they directly impinge onto the structures such as the fuel handling machine or the silicon doping

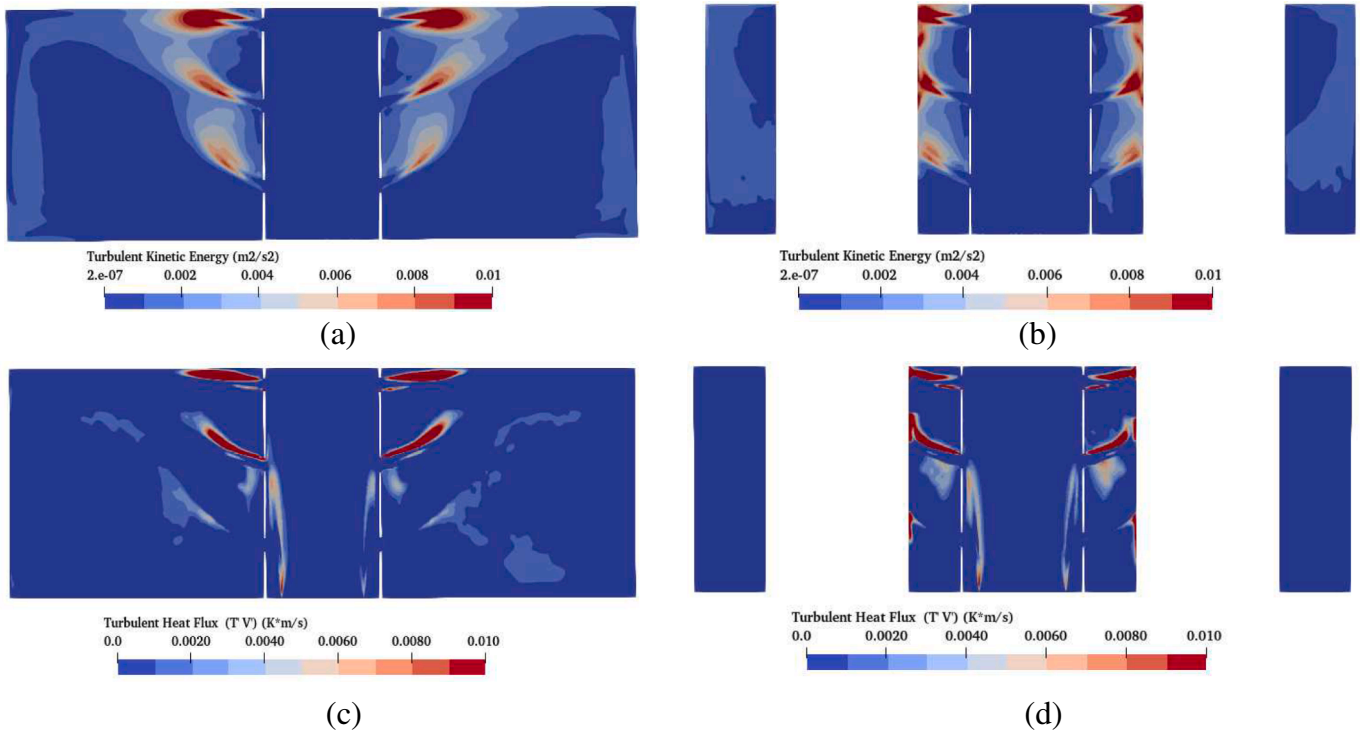

Fig. 10. Turbulent kinetic energy and turbulent heat flux distribution at planes along the free jet direction and along the jet interacting with IVFHM in the upper plenum region; (a and b) Turbulent kinetic energy, (c and d) Turbulent heat flux.

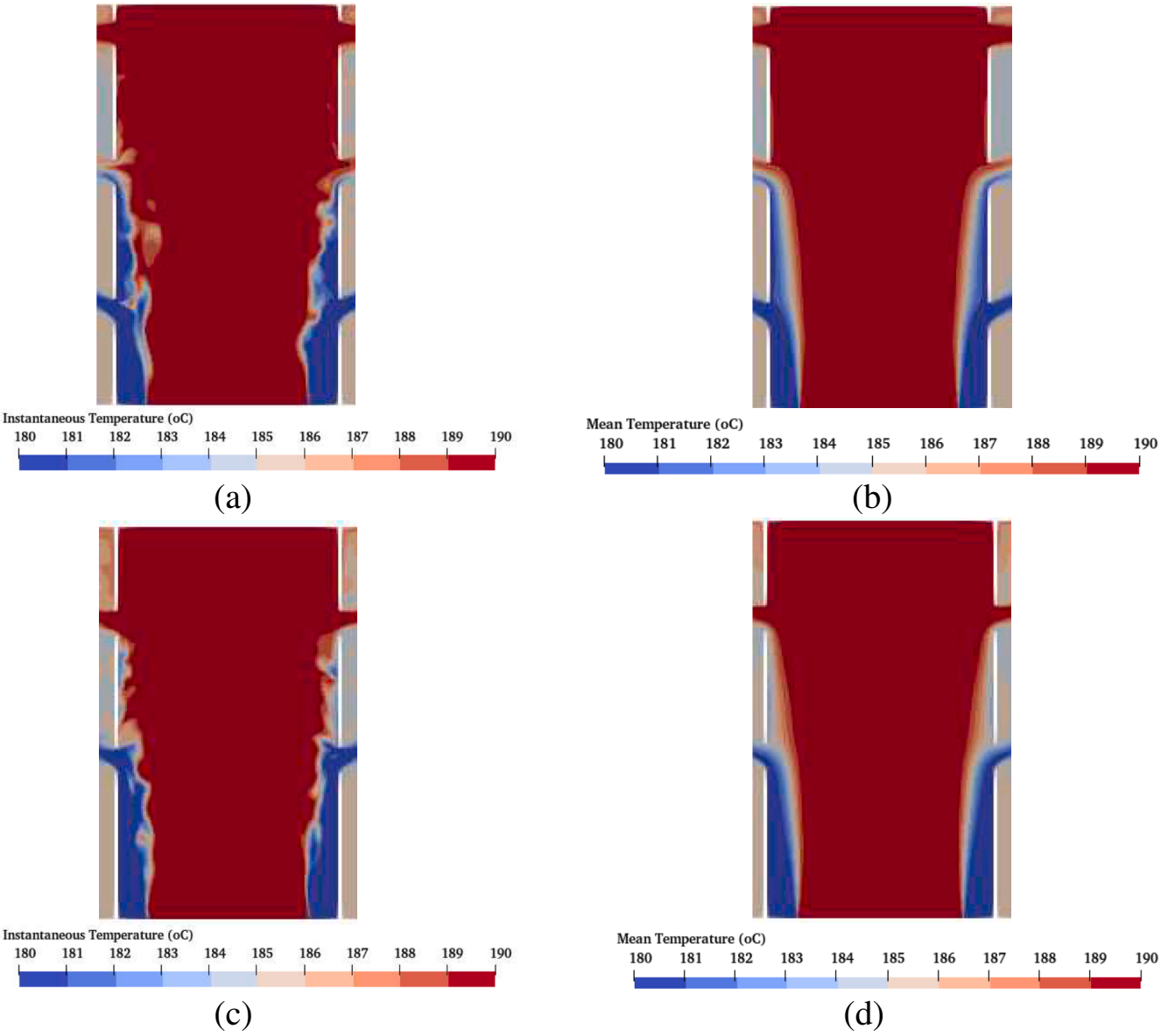

Fig. 11. Instantaneous and time averaged temperature distribution in the ACS region at planes along the direction of in-vessel fuel machine handling and the silicon doping device; (a and c) Instantaneous temperature profile, (b and d) Mean temperature profile.

device. In this section we consider the behavior of the free jets by studying the averaged statistics and relate them to visual observations.

The features of the jets can be obtained by analyzing the statistics of the flow along the jet trajectory in the radial direction. In Fig. 14 (b), the trajectory of the top, middle, and bottom jets is depicted, determined by tracing the path characterized by the maximum velocity of each jet. From the jet trajectories it is noticed that the top jet has a horizontal trajectory initially but due to the arrival of the middle jet, it suddenly shifts upwards by about one jet diameter before again maintaining a horizontal trajectory. The middle has the longest core trajectory which is inclined upwards. After its merging with the top jet, it turns into a horizontal trajectory. The bottom jet has a similar trajectory as the middle jet, inclined upwards initially and after merging with the second jet it bends horizontal. The jet trajectories can be visualized through the Fig. 14(a).

Fig. 15 illustrate the contour and radial profile of the mean temperature and velocity distribution for the free jets. The left panel displays the mean velocity with sub-figure (a) showcasing the whole field mean velocity contour and sub figures (c, e, and g) display the radial distribution of the mean velocity at several locations at jet trajectory, s which is defined as

$$s_n = s_{n-1} + \left((x_n - x_{n-1})^2 + (y_n - y_{n-1})^2\right)^{1/2} \tag{5}$$

Here s_n represents the distance between the points (x_n, y_n) and (x_{n-1}, y_{n-1}) at the jet trajectory. The coordinate (x_n, y_n) represents the local coordinate at the jet trajectory. The right panel of the figure shows similar a distribution but for mean temperature. The radial distributions are plotted up to $s/d = 7.0$, as beyond that point the temperature and the velocity become essentially uniform.

It can be seen from the figure that the top jet issues hotter fluid than that of the surroundings, the bottom colder fluid, and the middle mostly hotter but some colder at the lower part of the jet, see Fig. 15(b). The temperature profiles behave as expected, being the highest (lowest for the bottom) initially but the peak at the center reduces while the thermal boundary later expands. The center of the top jet drifted sideways whereas the other two jets largely retain their central position. Initially $(s/d < 4.0)$ the surrounding fluid remains at a similar temperature; the

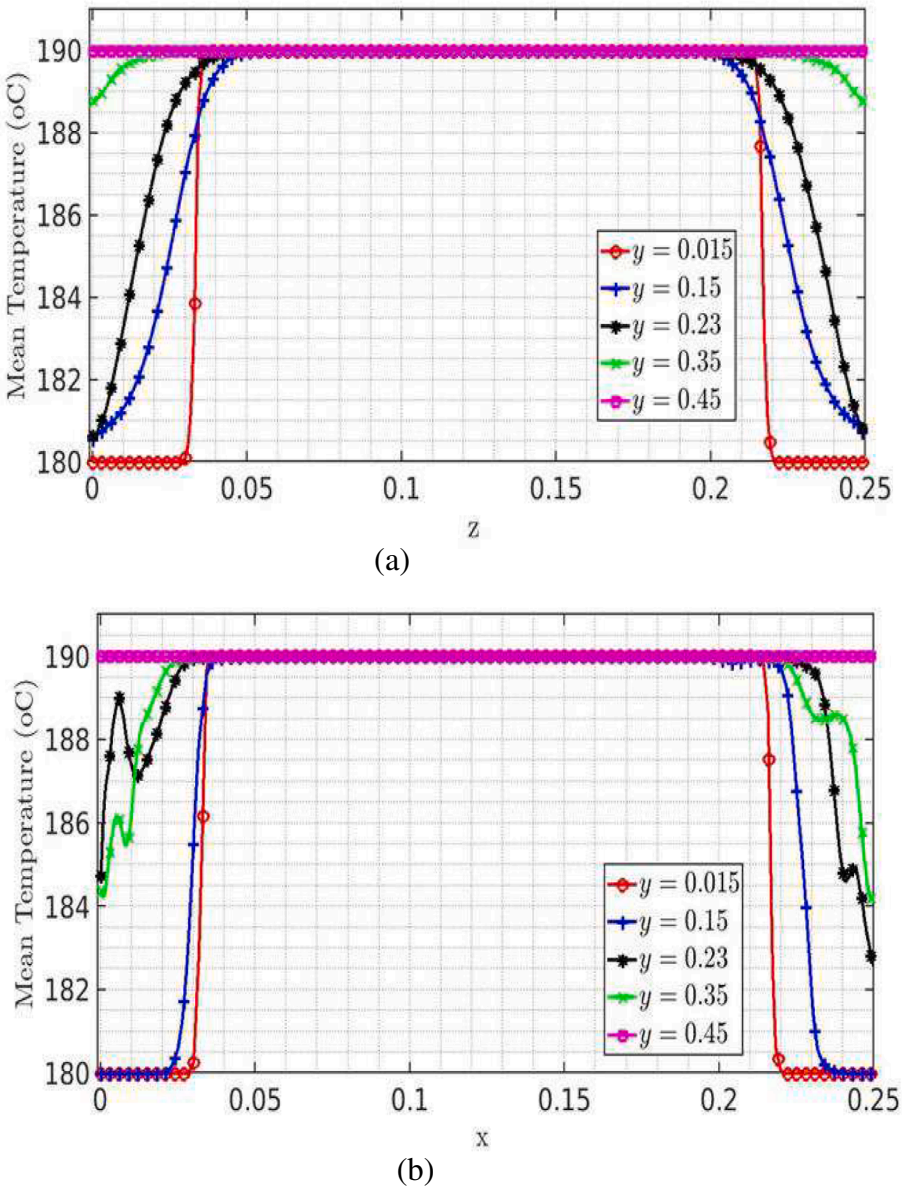

Fig. 12. Time averaged temperature distribution at various heights within the above core structure region focused on the direction of jet interacting with (a) In-vessel fuel handling and (b) SD device. x, y and z are in meters.

significant changes occur later which uplift the over temperature distribution.

In term of the velocity, the maximum velocity occurs at the center of the jet, which gradually decreases while the mixing layer expands as one move away from the jet source. There is a slow background velocity initially in the top two jets, but away from the jet sources ($s/d > 4.0$), the background velocity increases to a significant value. This occurs when the top and the middle jets merge. The background velocity for the bottom jet is on the other hand higher initially but becomes slower at later stages.

Fig. 16 illustrates the turbulent kinetic energy distribution for the jets. The radial profiles are plotted at several locations along the jet trajectory. There are clearly two peaks in the TKE profiles, one in each shear layer. The value of these peak is initially relatively low, but it increases as moving away from the jet, reaching their maximum value somewhere in the $s/d = 2.0$ or $s/d = 3.0$ region. These peaks then converge forming a new peak at the center of the jet while it gradually decays further downstream. This observation is further expressed by the contour plots in subfigure (a) of the figure, allowing for a visual representation of the TKE dynamics. The contour plots provide a clear depiction of the spatial evolution of TKE, emphasizing the presence of heightened energy levels in the shear layer region and their subsequent dissipation in the mixing region. The overall behavior of the free jets is qualitatively similar to typical rounded jet flows found in the literature, although the interaction with other jets prevents the formation of the self-similar region (Zhou et al., 2001; Ghaisas et al., 2015).

Fig. 17 shows the streamlines for each individual jet of the quarter portion of the upper plenum region. The streamlines which are calculated using the mean velocity presents the flow behavior of the rounded jets and their effects in the upper plenum region. For the sake of clarity, the streamlines are only plotted for the quarter portion of the upper plenum region. The jets are annotated are R-1, 2, 3, 4, 5 (five rows in the barrel wall); J-1, 2 (two jets in each row in the quarter portion of the upper plenum region).

It is interesting to see significantly different behaviors between the different jets, which is largely influenced by the location and angle of the

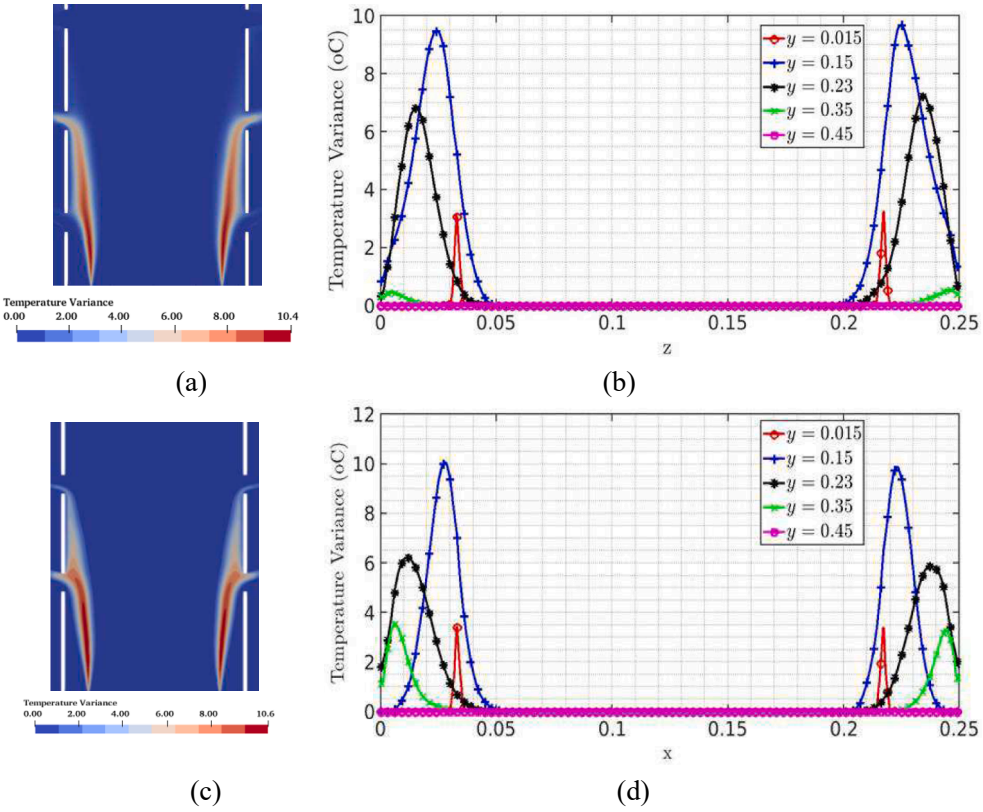

Fig. 13. Contours and radial distributions of temperature variance in the above core structure region along the IVFHM and SD devices direction; (a and c) Contour plots shows the whole field distribution; (b and d) Radial profiles show the distribution at different heights in the above core structure region in the direction of the IVFHM and SD devices;

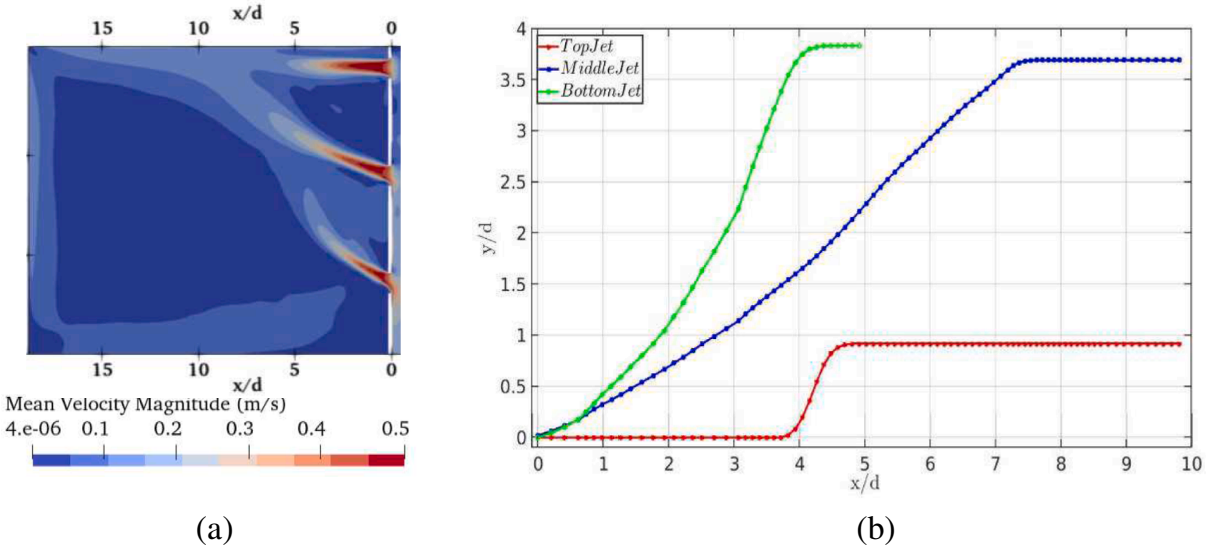

Fig. 14. Contours and the jet trajectories; (a) contours shows the whole region mean velocity distribution in the direction of free jet; (b) Radial profile shows the top middle and bottom jet trajectories, x and y are the local coordinate measured from the origin of the jet, d is the diameter of the jet/barrel hole.

jets. When the jets are angled towards the heat exchangers (i.e., the outlet of the flow), the streamlines are often shorter with less circulations, and vice versa. It can be seen that jets R-1 J-1; R-2 J-1; R-3 J-1 and R-4 J-1 have significantly longer paths. In contrast, the jets R-1 J-2; R-2 J-2; R-3 J-2 and R-4 J-2 which are oriented towards to the heat exchanger have formed much shorter circulation loop, only near the heat exchanger area before the flow enters into the heat exchanger. It is also observed that the first and second rows (rows starting from the top) of jets are largely horizontal, whereas the third forth and five rows jet display an inclined nature. The fluid in these rows moves upwards direction, contributing significantly to the vertical circulation. This behavior can be particularly noticed in the rows R-3; R-4 and R-5 jets. In

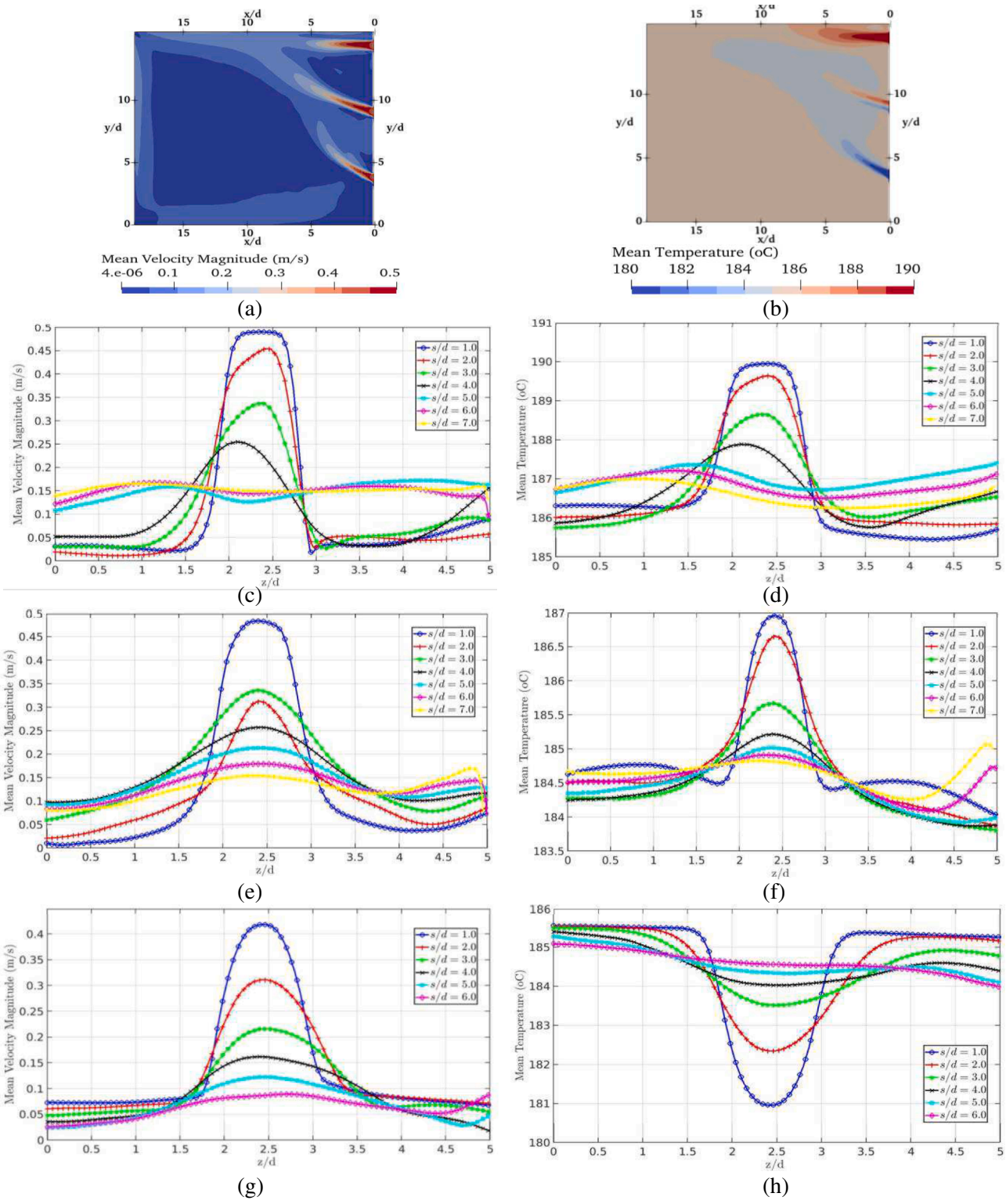

Fig. 15. Contours and the radial distribution of the mean velocity magnitude and mean temperature; (a and b) contours show the whole region mean velocity and mean temperature distribution in the direction of free jet; (c, d, e, f, g and h) Radial profile shows the distribution close to the top, middle and bottom jet followed by the jet trajectory.

summary, the orientation and position of the jets along the barrel wall in the upper plenum region of the E-SCAPE facility have a strong impact on the circulation patterns.

4. Conclusion

The paper presented a large eddy simulation of the upper plenum region of E-SCAPE, a test facility for a future LMFR. The results show interesting observations on the flow behaviors under the normal operating conditions, which represent forced convection flows. The model

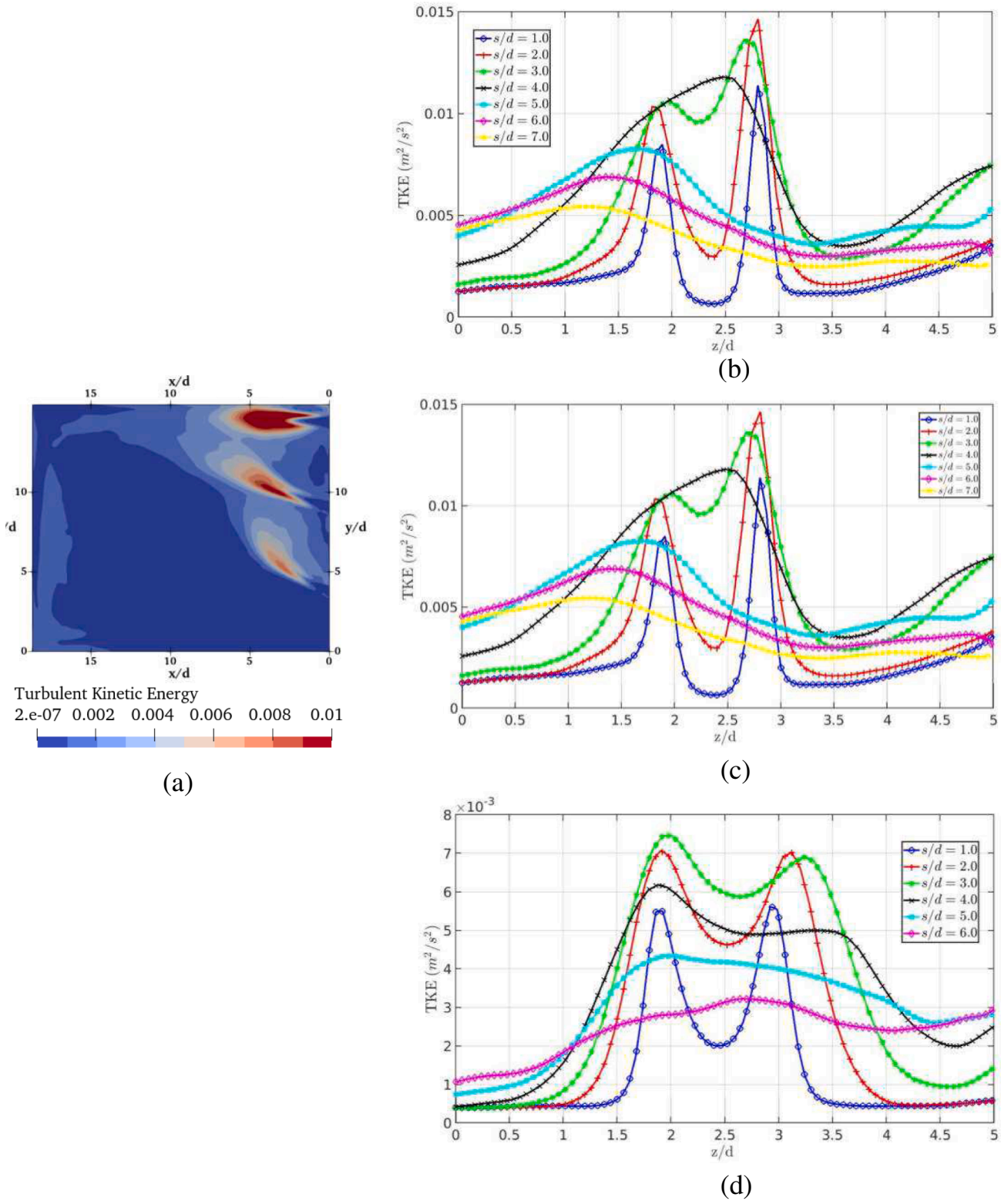

Fig. 16. Contours and the radial distribution of the turbulent kinetic energy; (a) contours shows the whole region TKE distribution in the direction of free jet; (b, c and d) Radial profile shows the distribution close to the top middle and bottom jet followed by the jet trajectory, d is the diameter of the jet inlet.

developed incorporated a porous media approach incorporating momentum source terms for the above core structure to account for the pressure losses in this region, which significantly reduce computational cost for the model overall. There are partially validated against experimental data, albeit with a small offset for the temperature. Limited experimental data prevented a more comprehensive validation.

The conclusions are made for three different regions within the E-SCAPE facility (i) The overall flow behavior in the upper plenum region (ii) thermal instability within the Above Core Structure region and (iii) the nature of the rounded jet in the free direction.

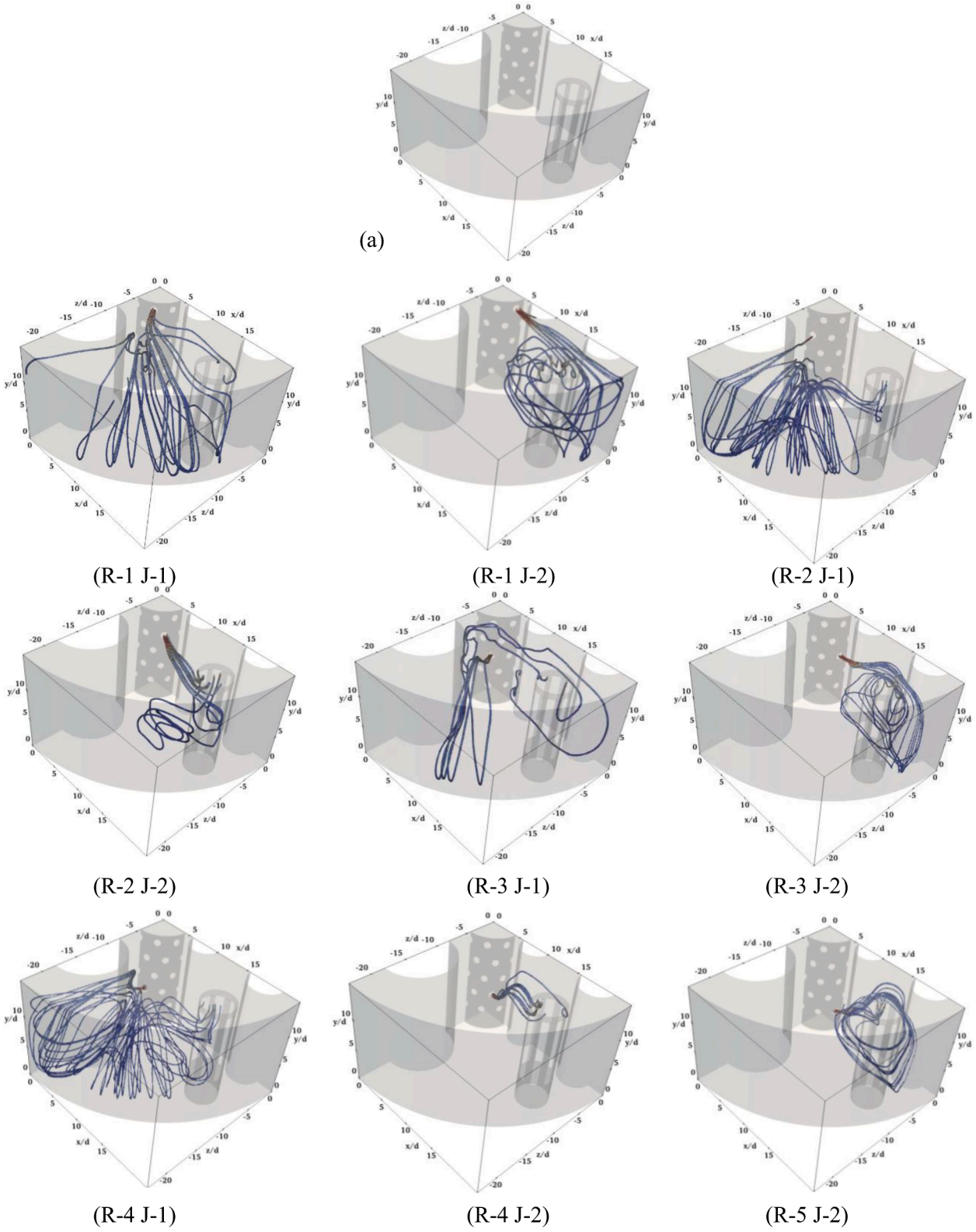

Fig. 17. Streamlines computed by using the mean velocity magnitude, originating from the jet .
Source in the upper plenum region; Rows R-1, 2, 3, 4, 5 represent the rows of the barrel holes (rows starting from the top), and J-1, 2 denotes the jet or barrel holes numbers

A uniform temperature distribution has been observed across the height of the upper plenum region under the normal operations attributed to large-scale circulations driven by the jets from the barrel holes. A slightly non-uniform temperature has also been observed close to the barrel wall region due to the influence of the lower jets carrying the cold liquid metal. Furthermore, the regions of lower temperature fluid are identified where the large circulation is blocked by the component within the E-SCAPE facility. These key features were also captured in

RANS simulations.

The instantaneous and the statistical analysis of temperature reveals strong temperature fluctuations within the above the core structure region due to the cold/hot fluid interactions. This is likely related to KH instability occurring in the mixing layer. The mean temperature however shows the presence of the smooth mixing layers at this region.

The flow from the barrel enters the upper plenum through barrel holes in the forms of complex jets. The jets at the top sections are issued largely horizontally whereas those away from this region angle upwards which help to create a strong vertical circulation. Jets directed towards the heat exchangers may directly exit the domain quickly whereas other jets would take long circulations which help the mixing. The free jets largely behave as a standard jet with minimum influence from the surrounding background flows until at a later stage $(s/d > 4.0)$. The observations in this study help to understand the fundamentals of the E-SCAPE facility's jet behavior.

CRediT authorship contribution statement

Ashish Saxena: Writing – original draft, Software, Methodology, Investigation, Formal analysis, Data curation. **Matthew Falcone:** Writing – review & editing, Software, Methodology, Investigation. **Shuisheng He:** Writing – review & editing, Supervision, Funding acquisition, Conceptualization.

Declaration of competing interest

The authors declare that they have no known competing financial interests or personal relationships that could have appeared to influence the work reported in this paper.

Data availability

Data will be made available on request.

Acknowledgements

The present work was funded by the Department of Business, Energy and Industry Strategy (BEIS) of the UK (Ref 1659/10/2018) and EPSRC (EP/T002395/1). This work used the ARCHER-2 UK National Supercomputing Service (http://www.archer2.ac.uk), provided via the UK Turbulence Consortium (grant EP/R029326/1).Additional funding was also received from CCP-NTH EP/T026685/1. The authors would like to thank Dr. Juan Uribe from EDF Energy for their assistance. The authors extend their gratitude to the University of Wisconsin, specifically to Mark Anderson, Nicholas Thoreson, and Ian Jentz, for their invaluable support in this project.

Appendix A:. Overall flow behavior of the upper plenum region based on the RANS simulation

In this section, we present the results obtained from the RANS simulations with the same boundary conditions as reported in Section 2.2. The $k-\epsilon$ turbulence model was used to model the Reynolds stresses using the same mesh as the LES case. The temperature and velocity profiles at various planes in the upper plenum region are presented in Figure A1. The left panel of the figure illustrates the temperature profile along the direction of the free jet (Figure A1(a)), the IVFHM direction (Figure A1(c)), and the direction of the silicon doping device (Figure A1(e)). Conversely, the right panel depicts the velocity profile in the same directions. The results indicate a largely uniform temperature along the height of the upper plenum, indicating thermal mixing phenomena within the region. Additionally, examination of the velocity distribution reveals the presence of a large-scale circulation, which play a significant role in facilitating thermal mixing within the upper plenum region.

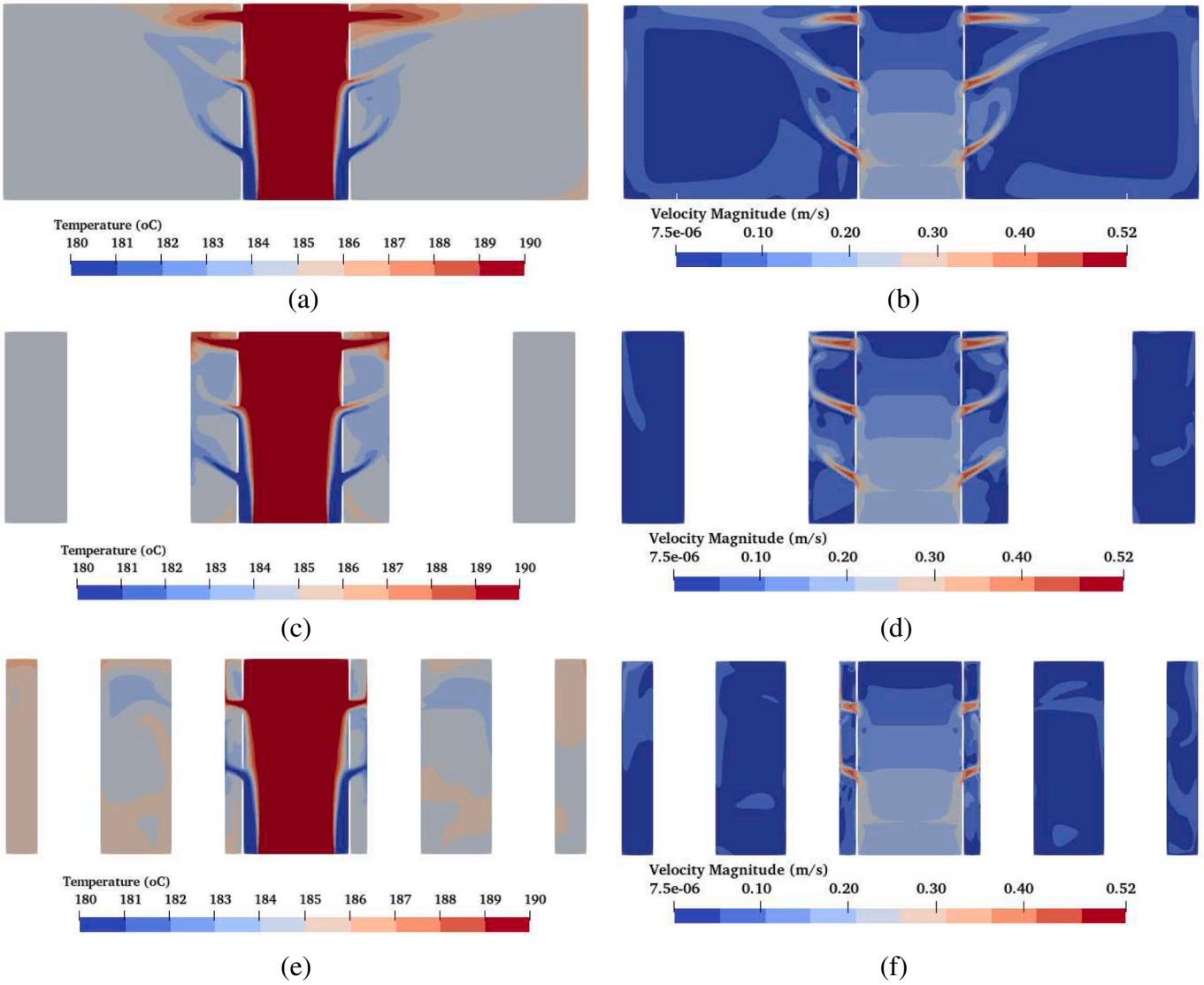

Fig. A1. Temperature and velocity at a plane along the free jet direction; along the IVHFM direction and along the SDs direction; (a, c and e) Temperature profile, (b, d and f) Velocity magnitude profile. Results are based on the RANS simulations.

The temperature and velocity distributions across the horizontal plane at various heights of the upper plenum are presented in Figure A2. In Figure A2 (a-1, a-2, and a-3), it's evident that the upper plenum region exhibits a predominantly uniform temperature distribution. However, a non-uniform temperature distribution is observed near the barrel jets in the middle of the upper plenum region, as shown in Figure A2 (a-2). This phenomenon is attributed to cooler fluid transported by the lower jets, which angle upwards and retain significant upward momentum. This suggests that both lower and upper jets play a significant role in the large-scale circulation in forced convection scenarios. Furthermore, subfigures (b-1), (b-2), and (b-3) illustrate the velocity distribution at different horizontal planes within the plenum. Impinging jets on the silicon doping devices and IVFHM are identified as potential areas of thermal striping. Additionally, flow separation is observed around cylindrical surfaces, particularly the silicon doping device, pumps, and IVFHM.

These results show that the RANS simulation can capture many of the overarching flow physics in the upper plenum region of the E-SCAPE facility that were observed in the LES simulation.

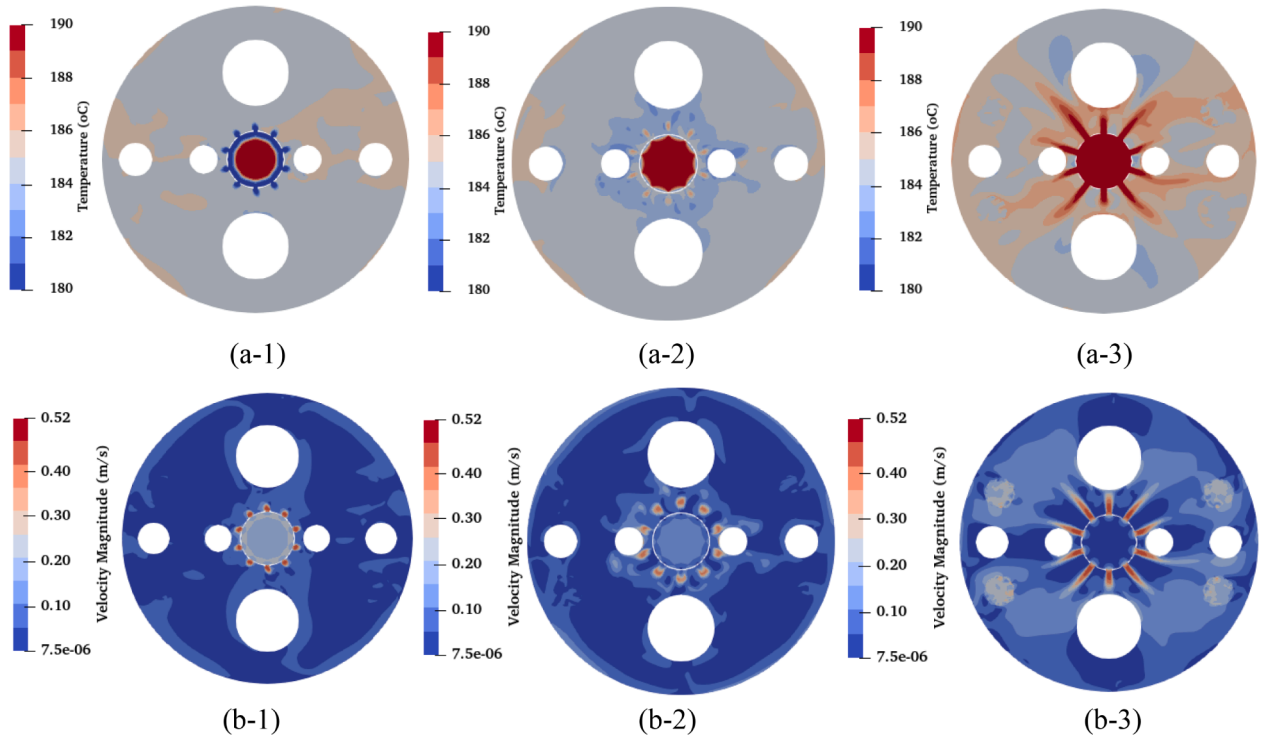

Fig. A2. Temperature and velocity distribution at different horizontal levels of the upper plenum; (a-1), (a-2) and (a-3) Temperature distribution; (b-1), (b-2) and (b-3) Velocity magnitude distribution. Results are based on the RANS simulations.

References

Angeli, D., Fregni, A., Stalio, E., 2019. Direct numerical simulation of turbulent forced and mixed convection of LBE in a bundle of heated rods with P/D = 1.4. Nucl. Eng. Des. 355, 110320.

Celik, I.B., Cehreli, Z.N., Yavuz, I., 2005. Index of resolution quality for large Eddy simulations. J. Fluids Eng. 127, 949–958.

Celik, I.B., Klein, M., Janicka, J., 2009. Assessment measurement for LES applications. J. Fluids Eng. 131, 031102.

Chacko, S., Chung, Y.M., Choi, S.K., Nam, H.Y., Jeong, H.Y., 2011. Large-eddy simulation of thermal striping in unsteady non-isothermal triple jet. Int. J. Heat Mass Transf. 54, 4400–4409.

Choi, S.K., Lee, T.H., Kim, Y.I., Hahn, D., 2013. Numerical analysis of thermal stratification in the upper plenum of the MONJU fast reactor. Nucl. Eng. Technol. 45 (2), 191–202.

Choi, S.K., Kim, D.E., Ko, S.H., Lee, T.H., 2015. Large-eddy simulation of thermal striping in the upper plenum of the PGSFR. J. Nucl. Sci. Technol. 52, 878–886.

Code_Saturne version 6.0.5 practical user's guide, EDF R&D, 2019.

Fregni, A., Angeli, D., Cimarelli, A., Stalio, E., 2019. Direct numerical simulation of a buoyant triple jet at low-Prandtl number. Int. J. Heat Mass Transf. 143, 118466.

Ghaisas, S.N., Shetty, D.A., Frankel, S.H., 2015. Large eddy simulation of turbulent horizontal buoyant jets. J. Turbul. 16, 772–808.

Grötzbach, G., 2013. Challenges in low-Prandtl number heat transfer simulation and modelling. Nucl. Eng. Des. 264, 41–55.

Kawamura, H., Abe, H., Matsuo, Y., 1999. DNS of turbulent heat transfer in channel flow with respect to Reynolds and Prandtl number effects. Int. J. Heat Fluid Flow 20 (3), 196–207.

Kenjeres, S., Gunarjo, S.B., Hanjalic, K., 2005. Contribution to elliptic relaxation modelling of turbulent natural and mixed convection. Int. J. Heat Fluid Flow 26, 569–586.

Koloszar, L., Buckingham, S., Planquart, P., Keijers, S., 2017. Myrrha Foam: A CFD model for the study of the thermal-hydraulic behavior of MYRRHA. Nucl. Eng. Des. 312, 256–265.

Pope, S.B., 2000. Turbulent Flows. Cambridge University Press.

Roelofs, F., Gopala, V.R., Van Tichelen, K., Cheng, X., Merzari, E., Pointer, W.D. Status and future challenges of CFD for liquid metal cooled reactors. international conference on fast reactors and related fuel cycles: safe technologies and sustainable, Scenarios (FR13) Presentations, (p. v). International Atomic Energy Agency (IAEA): IAEA.

Roelofs, F., Shams, A., Otic, I., Böttcher, M., Duponcheel, M., Bartosiewicz, Y., Lakehal, D., Baglietto, E., Lardeau, S., Cheng, X., 2015. Status and perspective of turbulence heat transfer modeling for the industrial application of liquid metal flows. Nucl. Eng. Des. 290, 99–106.

Roelofs, F., Gerschenfeld, A., Tarantino, M., Van Tichelen, K., Pointer, W.D., 2019. Thermal-Hydraulic Challenges in Liquid-Metal-Cooled Reactors, 17–43. Woodhead Publishing.

Shams, A., Roelofs, F., Baglietto, E., Lardeau, S., Kenjeres, S., 2014. Assessment and calibration of an algebraic turbulent heat flux model for low-Prandtl fluids. Int. J. Heat Mass Transf. 79, 589–601.

Sobolev, V., 2011. Database of thermophysical properties of liquid metal coolants for GEN-IV. Technical Report SCK•CEN Belgian Nuclear Research Centre.

Tichelen, K.V., Mirelli, F. Thermal-hydraulic experiments in the lbe-cooled scaled pool facility E-SCAPE, SESAME International Workshop Patten, Netherlands, 19-21, 2019.

Tichelen, K.V., Mirelli, F., Greco, M., Viviani, G., 2015. E-SCAPE: A scale test facility for liquid metal, pool-type reactor thermal hydraulics investigations. Nucl. Eng. Des. 290, 65–75.

Todreas, N.E., Kazimi, M.S. Nuclear systems I, Taylor & Francis Group, 1990.

Todreas, N.E., Kazimi, M.S. Nuclear Systems II, Taylor & Francis Group, 2001.

Toti, A., Vierendeels, J., Belloni, F., 2018. Extension and application on a pool-type test facility of a system thermal-hydraulic/CFD coupling method for transient flow analyses. Nucl. Eng. Des. 331, 83–96.

Visser, D.C., Roelofs, F., Mirelli, F., Tichelen, K.V., 2020. Validation of CFD analyses against pool experiments E-SCAPE. Nucl. Eng. Des. 369, 110864.

Visser, D.C., Keijers, S., Lopes, S., Roelofs, F., Tichelen, K.V., Koloszar, L., 2020. CFD analyses of the European scaled pool experiments E-SCAPE. Nucl. Eng. Des. 358, 110436.

Wang, M., Chen, J., Zhang, D., Zhang, J., Tian, W., Su, G.H., Qiu, S., 2020. Numerical study on the thermal stratification characteristics in the upper plenum of sodium-cooled fast reactor (SFR). Ann. Nucl. Eng. 138, 107222.

Yahya, S.M., Anwer, S.F., Sanghi, S., 2012. Performance of different SGS models of LES for low mach number channel flow. Procedia Eng. 38, 1192–1208.

Zhou, X., Luo, K.H., Williams, J.J.R., 2001. Study of density effects in turbulent buoyant jets using large-eddy simulations. Theor. Comput. Fluid Dyn. 15, 95–120.